PROCEEDINGS OF SPIE

SPIEDigitalLibrary.org/conference-proceedings-of-spie

Conformational equilibrium analysis of mCerulean3–linker–mCitrine constructs using time-resolved fluorescence measurements in controlled environments

Clint McCue, Sarah Mersch, Sarah Bergman, Erin Sheets, Ahmed Heikal

Clint McCue, Sarah A. Mersch, Sarah Bergman, Erin D. Sheets, Ahmed A. Heikal, "Conformational equilibrium analysis of mCerulean3–linker–mCitrine constructs using time-resolved fluorescence measurements in controlled environments," Proc. SPIE 12681, Ultrafast Nonlinear Imaging and Spectroscopy XI, 1268107 (5 October 2023); doi: 10.1117/12.2679719

SPIE.

Event: SPIE Optical Engineering + Applications, 2023, San Diego, California, United States

Invited Paper

Conformational equilibrium analysis of mCerulean3–linker–mCitrine constructs using time-resolved fluorescence measurements in controlled environments

Clint McCue[§], Sarah A. Mersch[§], Sarah Bergman, Erin D. Sheets, and Ahmed A. Heikal*

Department of Chemistry and Biochemistry, Swenson College of Science and Engineering, University of Minnesota Duluth, Duluth, MN, USA

[§] Coauthors contributed equally to this manuscript.

* Corresponding Author: Ahmed A. Heikal (aaheikal@d.umn.edu, 218-726-7036)

ABSTRACT

Macromolecular crowding and ionic strength in living cells influence a myriad of biochemical processes essential to cell function and survival. For example, macromolecular crowding is known to affect diffusion, biochemical reaction kinetics, protein folding, and protein-protein interactions. In addition, enzymatic activities, protein folding, and cellular osmosis are also sensitive to environmental ionic strength. Recently, genetically encoded mCerulean3-linker-mCitrine constructs have been developed and characterized using time-resolved fluorescence measurements as a function of the amino acid sequence of the linker region as well as the environmental crowding and ionic strength. Here, we investigate the thermodynamic equilibrium of structural conformations of mCerulean3-linker-mCitrine constructs in response to the environmental macromolecular crowding and ionic strength. We have developed a theoretical framework for thermodynamic equilibrium of the structural conformations of these environmental sensors. In addition, we tested these theoretical models for thermodynamic analysis of these donor-linker-acceptor sensors using time-resolved fluorescence measurements as a function of the amino acid sequence of the linker region. Employing ultrafast time-resolved fluorescence measurements for gaining thermodynamic energetics would be helpful for Förster resonance energy transfer (FRET) studies of protein-protein interactions in both living cells and controlled environments.

Keywords: Time-resolved fluorescence, FRET, donor-linker-acceptor, mCerulean3, mCitrine, macromolecular crowding, ionic strength, chemical equilibrium.

1. INTRODUCTION

Macromolecular crowding influences many biological processes in living cells including transport, biochemical reaction kinetics, enzyme activity, protein folding, and protein-protein interactions [1-3]. In addition, ionic strength is also critical for the structure-function relationship of proteins, enzymatic activities, and cellular osmosis [4-6]. Noninvasive, quantitative investigations of environmental crowding and ionic strength, however, are challenging due to their site specificity, heterogeneity, and dynamic nature.

Boersma and coworkers have developed genetically encoded donor-linker-acceptor protein constructs for site-specific environmental sensing for both macromolecular crowding [7-9] and ionic strength [10]. The environmental sensitivity of these constructs, based on the amino acid sequence of the linker region, can be quantified using time-resolved fluorescence measurements of the Förster resonance energy transfer (FRET) efficiency from the donor to the acceptor as a function of environment [11-16]. FRET is a non-radiative energy transfer process from the donor to an acceptor within ~10 nm distance, which is commonly considered a "molecular ruler" for protein-protein interactions and structural conformational studies [17, 18]. The FRET efficiency in donor-linker-acceptor constructs is sensitive to the donor-acceptor distance, relative dipole moment orientation, and spectral overlap of both the donor and acceptor proteins [17, 19]. The ability to

Ultrafast Nonlinear Imaging and Spectroscopy XI, edited by Zhiwen Liu, Demetri Psaltis, Kebin Shi, Proc. of SPIE Vol. 12681, 1268107
 · 0277-786X · doi: 10.1117/12.2679719

quantify distance between the proteins in these constructs allows for high resolution environmental sensing of either crowding or ionic strength.

Using time-resolved fluorescence measurements of the donor in the presence and absence of the acceptor as a point of reference, Heikal and coworkers have used these donor-linker-acceptor constructs as model systems for developing new experimental approaches such as time-resolved anisotropy [11, 12, 20] and fluorescence correlation spectroscopy [21] for FRET analysis and protein-protein interaction studies [15]. For crowding sensors with neutral linker amino acid sequences of varied length and flexibility, it was hypothesized that steric hindrance in a crowded environment would force the donor closer to the acceptor, which increases the FRET efficiency as the donor-acceptor distance decreases [11, 12, 16]. This hypothesis was tested on a number of crowding sensors such as G12, G18, E6, E6G2, and GE [7, 16] in controlled Ficoll-70 (a crowding agent) solutions. For ionic strength sensors such as RD, KE, and RE [10, 13, 15, 20], however, the linker region consists of two oppositely charged alpha helices where their electrostatic interactions are sensitive to the environmental ionic strength. For these ionic strength sensors, therefore, it was hypothesized that as the ionic strength increases, Debye ionic screening of the dissolved ions will reduce the electrostatic interactions between the two charged alpha helices and therefore increase the donor-acceptor distance and reduce the FRET efficiency [10, 13, 20].

In this contribution, we investigate the thermodynamic equilibrium and energetics associated with the conformational changes of selected mCerulean3-linker-mCitrine constructs in response to both environmental ionic strength (e.g., RD sensor) and macromolecular crowding (e.g., G12, G18, E6, and GE sensors, Table 1). We also provide a theoretical framework for using previously reported time-resolved fluorescence measurements on these sensors to elucidate the equilibrium constants and Gibbs free energy changes associated with their structural conformations in response to the environmental ionic strength (potassium chloride, KCl) and crowding (Ficoll-70 as a crowding agent). Two different approaches were also discussed for calculating the equilibrium constant using time-resolved fluorescence measurements of an ensemble of two different conformational distributions of donor-linker-acceptor constructs. These thermodynamic quantities were calculated for these environmental sensors as a function of KCl and Ficoll-70 concentrations as well as the number of amino acids in the linker region. The thermodynamic analyses were also discussed within the context of the published FRET efficiency and the donor-acceptor distance of these selected sensors.

2. THEORETICAL FRAMEWORK

For cleaved donor in the absence of tethered acceptor, the excited state population (N_1) of such a single species will change with time via fluorescence emission at a rate of k_D according to the following differential equation:

$$\frac{dN_1}{dt} = -k_D N_1 \tag{1}$$

Separating the variables and then integrating assuming the boundary conditions where at $t = 0$, $N_1 = N_0$, and at $t \to \infty$, $N_1 \to 0$), we obtain the following equation:

$$\int_{N_0}^{0} \frac{dN_1}{N_1} = -k_D \int_0^t dt \tag{2}$$

The solution of equation (2) is a single exponential decay at a rate constant of k_D, which can be written as:

$$N_1(t) = N_0 e^{-k_D t} \tag{3}$$

Since the fluorescence signal (F_1) is proportional to the number of molecules (N_1) in the excited electronic state, equation (3) can be rewritten as the corresponding fluorescence decay of the donor alone (F_D) such that:

$$F_D(t) = F_0 e^{-k_D t} \tag{4}$$

Where F_0 is the initial amplitude of the fluorescence decay at $t = 0$. Accordingly, the excited electronic state population of a fluorescent molecule (e.g., donor in the absence of an acceptor) will decay as a single exponential with a fluorescence decay rate depending on the chemical structure and the surrounding environment. Figure 1A (curve 1) shows the fluorescence decays of the donor alone (or cleaved G12 sensor) in PBS buffer.

In the presence of an acceptor that is tethered to the donor (i.e., intact sensor), however, the excited state population of the donor molecule will decay at the sum of the fluorescence decay rate (k_D) of the donor plus the energy transfer rate (k_{ET}) from the donor to the acceptor, where the corresponding differential equation can be written as following:

$$\frac{dN_1}{dt} = -k_D N_1 - k_{ET} N_1 = -\left(k_D + k_{ET}\right) N_1 \tag{5}$$

Here, we assumed that the whole excited-state population ensemble would undergo parallel decays via fluorescence decay (k_D) of the donor and energy transfer rate (k_{ET}) from the donor to the acceptor. Separating the variables and then integrating, $N_1 \to 0$; as $t \to \infty$ (where $t = 0$ is the moment at which the molecules is excited by a femtosecond laser pulse):

$$\int_{N_0}^{0} \frac{dN_1}{N_1} = -\left(k_D + k_{ET}\right) \int_{0}^{t} dt \tag{6}$$

Using the boundary conditions (at $t = 0$ of pulsed excitation, $N_1 = N_0$, at $t > 0$, at $t > \infty$, $N_1 = 0$), the solution of equation (6) is a single exponential decay at a rate constant of $k_D + k_{ET}$ which can be written as:

$$N_1(t) = N_0 e^{-(k_D + k_{ET})t} \tag{7}$$

Alternatively, the corresponding fluorescence of the donor in the presence of an acceptor, F_{DA}, will also decay as a single exponential (according to equation 7) such that:

$$F_{DA}(t) = F_0 e^{-(k_D + k_{ET})t} \tag{8}$$

Assuming a very efficient energy transfer ($k_{ET} \gg k_D$), the excited-state population of the donor, in the presence of an acceptor, will decay also as a single exponential with a fluorescence decay rate of approximately k_{ET}. For a single population of FRET pairs, where the excited donor undergoes both FRET and fluorescence, the donor's fluorescence will decay as a single exponential at the sum of rates, $k_{ET} + k_D$. However, time-resolved fluorescence of the donor in the presence of the acceptor (Figure 1A, Curve 2) shows that the single exponential fitting model does not satisfactorily describe the observed fluorescence decay as judged by both the residuals (Figure 1B and C) and the estimated χ^2–values.

Since an ensemble of FRET pairs undergoes thermal fluctuations, however, it is likely that a subpopulation of structural conformations would have unfavorable donor-acceptor distance or orientation parameter (*e.g.*, perpendicular dipole moments). This would lead to the presence of two conformations in the ensemble of FRET pairs that are thermally at equilibrium, where one subpopulation undergoes energy transfer (*e.g.*, collapsed) and another does not (*e.g.*, stretched) as described below.

In an ensemble of FRET pairs with two subpopulations at thermal equilibrium, one undergoing FRET (*e.g.*, collapsed, *C*) and another that does not (*e.g.*, stretched, *S*), the corresponding fluorescence decay of the donor in the presence of an acceptor can be written as a sum of Equations (4) and (8) such that:

$$F_{DA}(t) = \alpha_1 e^{-(k_D + k_{ET})t} + \alpha_2 e^{-(k_D)t} \tag{9}$$

Under this approximation, the FRETing subpopulation (collapsed conformation) will decay at a rate that is the sum $k_{ET} + k_D$ (first term), where the energy transfer rate (k_{ET}) can be determined. In addition, the second term of Equation (9) describes the non-FRETing subpopulation (stretched conformation) due to either unfavorable donor-acceptor distance or relative dipole moment orientations, where fluorescence of the donor will decay approximately at a rate of k_D. Such an assumption is supported by the observed time-resolved fluorescence of G12 ensemble in PBS buffer and the goodness (residuals, Figure 1B and C, and χ^2–values) of the biexponential fitting model.

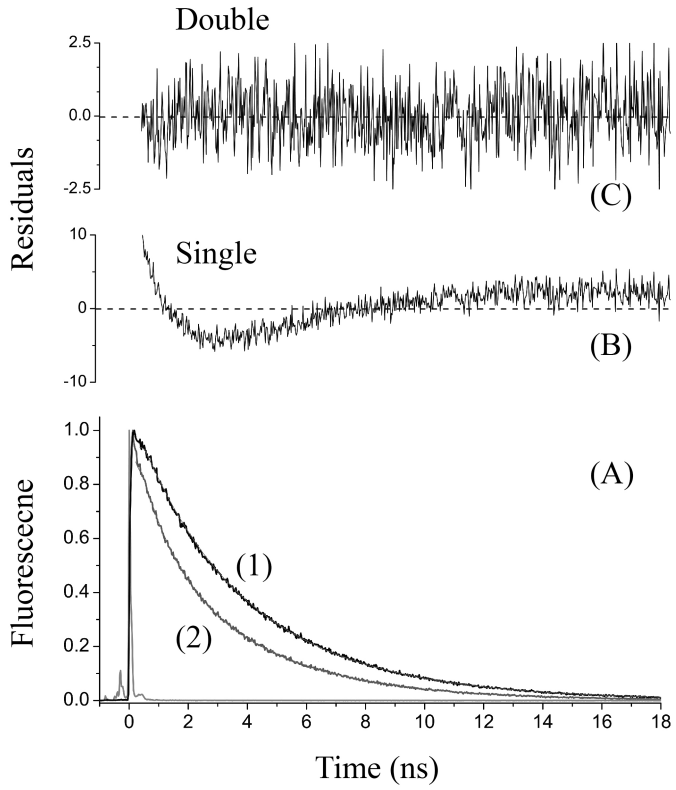

Figure 1: Representative time-resolved fluorescence of intact G12 sensor decays as a biexponential under 425-nm pulsed excitation of the donor (mCerulean3) in the presence of the acceptor (mCitrine). (A) The fluorescence decays of cleaved (curve 1) and intact (curve 2) G12 sensor are distinct due to FRET from the donor to the acceptor in mCerulan3-linker-mCitrine construct. The instrument response function of our inverted microscope based experimental setup (light gray curve) is also shown with pre-exponential satellites due to internal reflection of the microscope optics. The residual of the single (B) and double (C) exponential fitting curves are also shown as one criterion for the goodness of the fit in addition to the estimated χ^2 (data not shown).

Using time-resolved fluorescence techniques such as TCSPC, the observed biexponential fluorescence decay can be written generically in terms of the amplitude (α_i) and time constant (τ_i) associated with each i^{th} species (i = 1, 2) such as:

$$F_{DA}(t) = \alpha_1 e^{-t/\tau_1} + \alpha_2 e^{-t/\tau_2} \equiv \alpha_C e^{-t/\tau_{fast}} + \alpha_S e^{-t/\tau_{slow}} \quad (10)$$

Where α_1 and α_2 represent the population fraction of fast decay component (or collapsed conformation, α_C) and slow decay component (or collapsed conformation, α_S) respectively. For donor-linker-acceptor constructs, the energy transfer rate and therefore the FRET efficiency is expected to depend on the surrounding environment, the linker amino acid sequence, and the temperature.

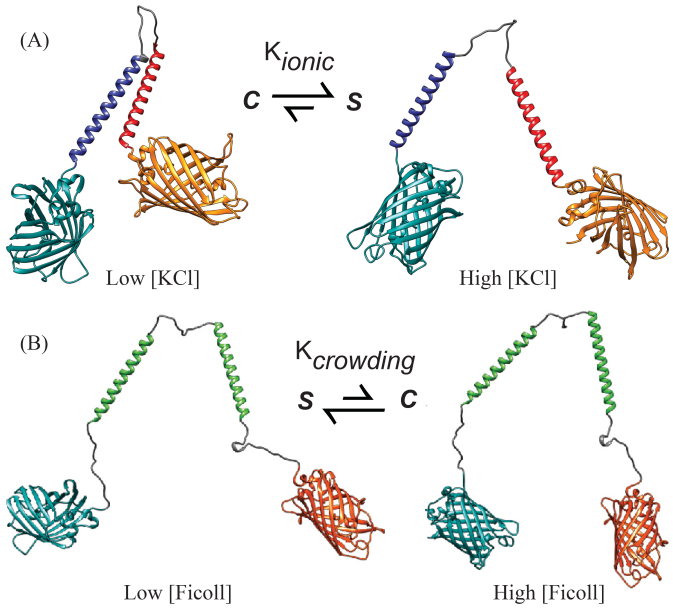

Figure 2: Hypotheses describing the conformational changes of ionic strength (RD) and crowding (G12, G18, E6, and GE) sensors in response to the environmental ionic strength. (A) As the ionic strength increases, ionic screening reduces the electrostatic interactions between the two oppositely charged alpha helices in RD resulting in a stretched conformation (*S*) and reduced donor-acceptor distance (i.e., lower FRET). (B) In crowded environments (*e.g.*, higher concentration of Ficoll-70 as a crowding agent), steric hindrance brings the donor and acceptor closer (collapsed conformation, *C*) in crowding sensors and therefore enhanced FRET efficiency. It is worth mentioning that each of these structural conformations (collapsed or stretched) may be considered as the center of a distribution (*e.g.*, Boltzmann distribution) in the ground electronic state of a given mCerulean3-linker-mCitrine construct.

Assuming an ensemble of mCerulean3-linker-mCitrine constructs, behaving as an ionic strength sensor (*e.g.*, RD) due to its oppositely charged alpha helices in the linker region, we hypothesize that there are two distributions of collapsed and stretched conformational subpopulations that exist at thermal equilibrium (Figure 2A) such that:

$$C \underset{}{\overset{K_{ionic}}{\rightleftharpoons}} S \quad (11)$$

As the environmental ionic strength increases, the electrostatic interaction between the two oppositely charged alpha helices in RD will be reduced due to ionic screening (shielding), which will lead to a reduced donor-acceptor distance and therefore enhanced energy transfer efficiency. The equilibrium constant (*K*) of such an ensemble can be calculated in terms of the concentrations of both the stretched (*S*) and collapsed (*C*) conformations such that:

$$K_{ionic} = \frac{[S]}{[C]} \quad (12)$$

We can use time-resolved fluorescence of this ensemble of mixed conformations (equations 9 or 10) to approximately determine the relative populations (concentrations) of the collapsed and stretched conformations. In one approach, the observed biexponential fluorescence decay can be used to determine the fractional number of fluorescence photons emitted by each conformation (e.g., f_C or f_S) in the ensemble such that:

$$f_C = \frac{\alpha_1\tau_1}{\alpha_1\tau_1 + \alpha_2\tau_2} \propto \varphi_C[C] \tag{13}$$

and,

$$f_S = \frac{\alpha_2\tau_2}{\alpha_1\tau_1 + \alpha_2\tau_2} \propto \varphi_S[S] \tag{14}$$

In equations (13) and (14), the fluorescence signal emitted by a given species or conformation (*i.e.*, *C* or *S*) is proportional to the concentration and the fluorescence quantum yield (φ). Such an approach is routinely employed in chemical kinetics studies using steady-state spectroscopy (*e.g.*, using spectrofluorimetry) [22-24]. In this case, the corresponding equilibrium constant (*K*) can be rewritten as:

$$K^{a}_{ionic} = \frac{[S]}{[C]} = \frac{f_S}{f_C} = \frac{\alpha_2\tau_2}{\alpha_1\tau_1} \tag{15}$$

This approach is sound since the fluorescence signal is directly proportional to the concentration of given fluorophore (or conformation) under the same experimental conditions of illumination and detection. However, the fluorescence signal also depends on the fluorescence quantum yield (φ) of the fluorescence of a given chemical structure and surrounding environment, which is not accounted for by equation (15).

The second approach for using time-resolved fluorescence of a mixture of two conformations of donor-linker-acceptor constructs accounts for the difference in the quantum yield of the donor in the presence and absence of the acceptor. The fluorescence quantum yield (φ) of the donor in a collapsed conformation, for example, is proportional to the corresponding fluorescence lifetime (*i.e.*, $\varphi \propto \tau_i$). Therefore, to remove the influence of quantum yield on the collapsed and stretched conformations, the equilibrium constant (*K*) in this second approach can be rewritten in terms of the amplitude fraction of the observed biexponential decay such that:

$$K^{b}_{ionic} = \frac{[S]}{[C]} = \frac{f_S}{f_C} = \frac{\alpha_2}{\alpha_1} \tag{16}$$

In either approach, the corresponding Gibbs free energy change (ΔG^0) for equilibrium can be calculated using the estimated equilibrium constant in both approximations such that:

$$\Delta G^{\circ}_{i} = -RT\ln(K_i) \tag{17}$$

Where "*i*" can be either "*a*" or "*b*" for an ionic strength donor-linker-acceptor sensor, depending on the employed approach for using the time-resolved fluorescence measurements of a mixture of two conformations (i.e., collapsed and stretched) to determine the corresponding rate constant (*K*).

It is worth mentioning that the conformational changes of crowding sensors (e.g., G12, G18, E6, and GE) in response to the concentrations of the crowding agent (e.g., Ficoll-70) follows a different thermodynamic equilibrium as shown in Figure 2B. In the crowding sensors case, it is hypothesized that steric hindrance in crowded environment would force the donor closer to the acceptor, which increases the FRET efficiency as the donor-acceptor distance decreases (Figure 2B).

3. MATERIALS AND METHODS

Isolation and purification of the mCerulean3-linker-mCitrine constructs from their respective DNA were described in detail elsewhere [7, 9, 11]. The amino acid sequences of the linker region in RD (ionic strength sensor with two oppositely charged alpha helices) [13, 20] as well as G12, G18, E6, and GE (crowding sensors with neutral alpha helices of varying length and flexibility) [11, 12, 16] are summarized in Table 1. As a control in the previous experimental studies on these sensors, enzymatic cleavage of the linker region using the serine protease Proteinase K was carried out to create mCerulean3 alone in the absence of the acceptor (*i.e.*, no FRET) [11-13, 16]. SDS-PAGE analysis was used to ensure complete cleavage of the linker region prior to experimentations.

The experimental setup for time-resolved fluorescence measurements has been described in great details elsewhere [12, 13, 16]. In these measurements, 425-nm laser pulses (4.2 MHz, ~120 fs pulse width) were used to excite the donor of mCerulean3-linker-mCitrine constructs for ionic strength (RD) and crowding (G12, G18, E6, and GE) sensing. The time-resolved fluorescence (475/50) was measured at magic angle (54.7°) polarized detection and time-correlated single-photon counting technique based on SPC-830 module (Becker & Hickl) [12, 13, 16]. The system was calibrated daily using coumarin-1 solution under the same experimental conditions. The measured fluorescence decays of both cleaved and intact sensors were deconvoluted with a computer-generated system response function and analyzed using SPCImage software (Becker & Hickl) [12, 13, 16].

Table 1: Linker sequences of mCerulean3-linker-mCitrine constructs of RD (ionic strength sensor) and G12, G18, E6, and GE (crowding sensors). The linker region of RD consists of two oppositely charged alpha helices as compared with the neutral linker region of varied length and flexibility of G12, G18, E6, and GE constructs.

Sensors	Amino Acid Sequence of the Linker Region	Number of Amino Acids
RD	–A$(AAAAR)_6$A$(GSG)_6$$(DAAAA)_6$A–	81
G12	–$(GSG)_{12}$–	36
G18	–$(GSG)_{18}$–	54
E6	–$(GSG)_6$A$(EAAAK)_6$A$(GSG)_6$–	68
GE	–A$(GSG)_6$$(EAAAK)_6A(GSG)_6A(EAAAK)_6$$(GSG)_6$A–	118

4. RESULTS AND DISCUSSION

4.1 Thermodynamic Analysis of Conformational Equilibrium of Ionic Strength RD Sensor

The linker region of RD consists of two oppositely charged alpha helices that connect the donor (mCerulean3) and the acceptor (mCitrine) together (Table 1). It was hypothesized that as the ionic strength increases, the electrostatic interaction between the two oppositely charged alpha helices in RD will be reduced due to ionic shielding, which will lead to a reduced donor-acceptor distance and therefore enhanced energy transfer efficiency [13, 20]. Time-resolved fluorescence of intact RD exhibits biexponential fluorescence decay in contrast to the cleaved (donor alone) counterpart, which decays satisfactorily as a single exponential (Figure 1). In addition, as the KCl concentration (ionic strength) increased, the energy transfer efficiency decreased and the donor-acceptor distance increased [13, 20], which supports the stated hypothesis.

We used the time-resolved fluorescence of RD [13] to calculate the corresponding equilibrium constant and the Gibbs free energy changes in NaPi buffer at room temperature and the results are shown in Figure 3. While there is a difference in the estimated equilibrium constant depending on the calculation approach, both values are positive while the fluorescence photons-based estimate (K = 14) is larger than the amplitude-based approach (K = 2) as shown in Figure 3A. In addition, the corresponding Gibbs free energy changes suggest that the collapsed conformation of RD in a buffer is more favorable regardless of the calculation approach for

the equilibrium constant. However, the estimated Gibbs free energy changes (–0.8 kJ/mol *versus* –6.2 kJ/mol) depends on how we calculate the equilibrium constant using observed time-resolved fluorescence of RD in a given environment. The results suggest a favorable collapsed conformation of RD in a buffer, which can be attributed to the electrostatic interaction between the two oppositely charged alpha helices in the linker region. In addition, the conformational change from collapsed to stretched structure of RD is also spontaneous, regardless of how we calculate the equilibrium constant using time-resolved fluorescence as outlined above.

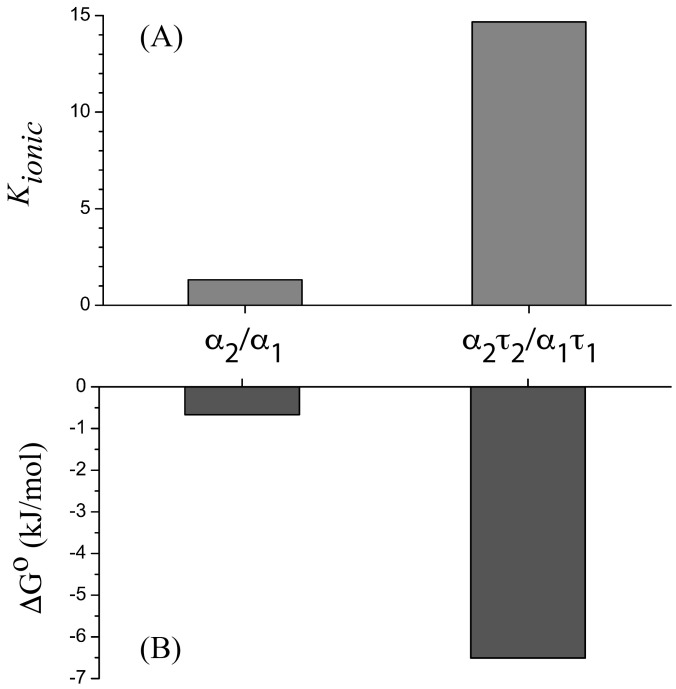

Figure 3: Different approaches for calculating the equilibrium constant and the Gibbs free energy of RD in NaPi buffer (pH 7.4). (A) The equilibrium constant (*K*) of an ionic strength sensor (RD) in NaPi buffer were calculated using both the amplitude fractions (α_2/α_1) and the fluorescence photons emitted by each conformation ($\alpha_2\tau_2/\alpha_1\tau_1$) based on the observed biexponential decay of the intact construct. (B) The corresponding Gibbs free energy changes (ΔG^0) of an ionic strength sensor (RD) in NaPi buffer were calculated using both approaches for determining the equilibrium constants as described in (A) at room temperature. The estimations of these thermodynamic quantities are based on time-resolved 1P-fluorescence measurements of the intact RD sensor [13].

It was also reported that the FRET efficiency (*i.e.*, sensitivity) of RD decreases as the environmental ionic strength increased in potassium chloride (KCl) solutions [13, 20]. It was hypothesized that as the ionic strength increases, the electrostatic interaction between the two oppositely charged alpha helices is reduced due to Debye ionic screening of the linker region, which leads to an enhanced donor-acceptor distance and therefore lower FRET efficiency [13, 20].

Using the reported time-resolved fluorescence parameters, we examined the thermodynamic equilibrium of RD in response to the environmental ionic strength in KCl solutions at room temperature. Here we used the amplitude ratio (α_2/α_1) based calculations to estimate the corresponding equilibrium constant of RD at a given KCl concentration. As shown in Figure 4, our analyses indicate that the Gibbs free energy (ΔG^0) change decreases as the KCl concentration (or ionic strength) increases. This suggests that the stretched

conformation of RD becomes more favorable as the environmental ionic strength increases, which agrees with our stated hypothesis.

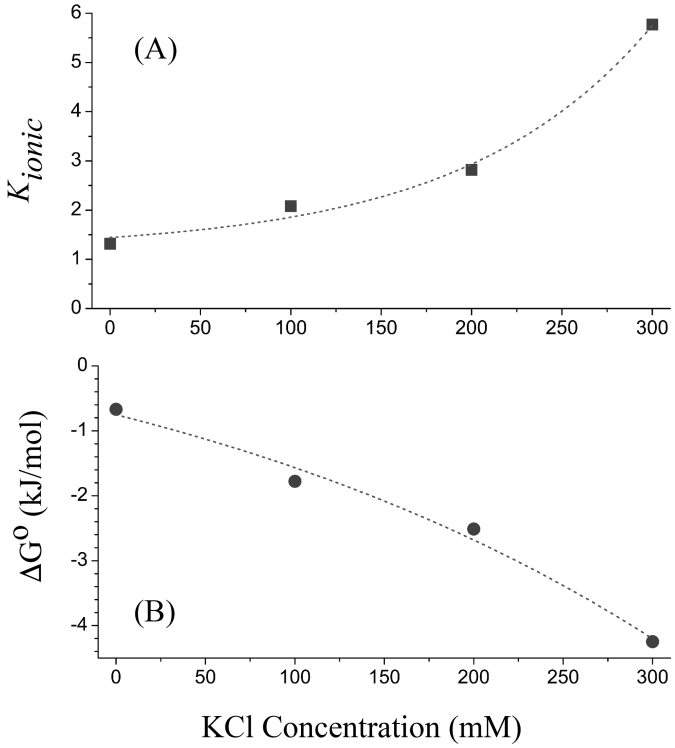

Figure 4: The estimated Gibbs free energy changes of intact RD decreases as the ionic strength (or KCl concentration) increases. The equilibrium constant (A) and the Gibbs free energy changes (B) of RD were calculated using the amplitude fractions (α_2/α_1) of the previously reported time-resolved fluorescence as a function of KCl concentration [13]. The dotted lines are shown here for eye guidance only with no theoretical basis.

4.2 Effect of Linker Amino Acid Sequence on their Thermodynamics Equilibrium of Crowding Sensors

Schwarz *et al*. [16] have investigated time-resolved fluorescence measurements of a family of mCerulean3-linker-mCitrine crowding sensors (namely, G12, G18, E6, and GE) in PBS buffer (pH 7.4) enriched with Ficoll-70 at different concentrations. The key difference between these crowding sensors is the amino acid sequence in the neutral linker region (Table 1), which also dictates it length and flexibility [7, 16]. It was hypothesized that sensors with short and flexible linker region will exhibit higher sensitivity to crowding and therefore enhanced FRET efficiency as measured using time-resolved fluorescence of the donor (mCerulean3) in the presence and absence of the acceptor (mCitrine). To test this hypothesis, time-resolved fluorescence measurements of the donor, in the presence and absence of the acceptor, were carried out using 425-nm pulsed laser excitation and the corresponding fluorescence signal was detected at a magic angle polarization as a function of the amino acid sequences of G12, G18, E6, and GE (Table 1).

It was reported that G12 and G18, with the most flexible linkers, showed the highest energy transfer efficiency (*i.e*., shortest donor-acceptor distance) as compared with GE sensor in a PBS buffer at room temperature (Table 1 for the linker sequence) [16]. For example, both G12 (E = 29%) and G18 (E = 27%) exhibited the highest energy transfer efficiency as compared with GE (E = 12%) sensor in buffer, Figure 5A, [12, 16].

To understand the underlying thermodynamic driving forces associated with these sensors in response to macromolecular crowding, we used the fitting parameters of the published time-resolved fluorescence of G12, G18, E6, and GE sensors to calculate the corresponding equilibrium constant ($K^b_{crowding}$, Figure 5B) and Gibbs free energy changes (ΔG^0, Figure 5C) as a function of the amino acid sequence. In these calculations, we employed the amplitude fraction ratios of the observed fluorescence decays of each sensor to calculate the corresponding equilibrium constant ($K = \alpha_1/\alpha_2$) in a given environment (Figure 5B). As shown in Figure 2 (*i.e.*, hypotheses), the equilibrium constant for crowding sensors ($K^b_{crowding}$) is the inverse of the corresponding the equilibrium constant for the ionic strength sensors (K^b_{ionic}), as the linker region is hypothesized to compress in response to environmental crowding (Figure 2B).

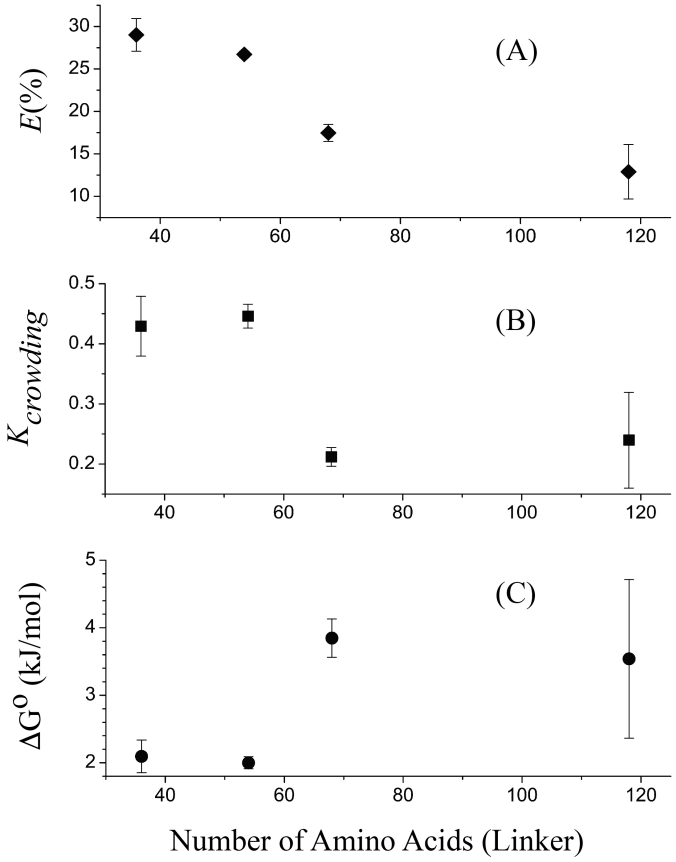

Figure 5: The estimated FRET efficiency (or sensitivity) is correlated with the equilibrium constant and the Gibbs free energy of the hypothesized conformational changes of G12, G18, E6, and GE crowding sensors with neutral linker region. (A) Previously reported FRET efficiency increases as the linker region becomes shorter and more flexible. These analyses are based on the previously published time-resolved 1P-fluorescence on the same sensors, where both G12 and G18 exhibited the highest energy transfer efficiency as compared with GE sensor [12, 16]. The amplitude-based equilibrium constant, (*i.e.,* α_1/α_2), (B) and the Gibbs free energy changes, ΔG^0, (C) of crowding sensors also help understand the conformational response (hence sensitivity) of crowding sensors as a function of the amino acid sequence of the linker region in PBS buffer at room temperature.

Figure 5 shows that G12 and G18 have relatively lower Gibbs free energy changes and therefore favorable collapsed conformation as compared with GE and E6 in PBS buffer. This trend can be understood in terms of the short and more flexible linker region of G12 and G18, which also validate the stated hypothesis above. In addition, the structure conformational equilibrium (stretched to collapsed) of these crowding sensors is not spontaneous (*i.e.*, $\Delta G^0 > 0$).

4.3 Concentration Effect of Ficoll-70 on their Thermodynamics Equilibrium of G12 Crowding Sensor

It was also hypothesized that the donor-acceptor distance will become smaller, and therefore the FRET efficiency will increase, as the concentration of the crowding agent increases. To test this hypothesis, the authors carried out time-resolved fluorescence of the donor, in the presence and absence of the acceptor, using 425-nm pulsed laser excitation and the emission was detected at a magic angle polarization as a function of Ficoll concentration [16]. It was reported that the FRET efficiency (sensitivity) of G12, G18, E6, and GE sensors increased as the concentration of Ficoll-70 increased. Such observations were interpreted in terms of the crowding-induced steric hindrance that forces the donor and acceptor closer, which validates the stated hypotheses [12, 16].

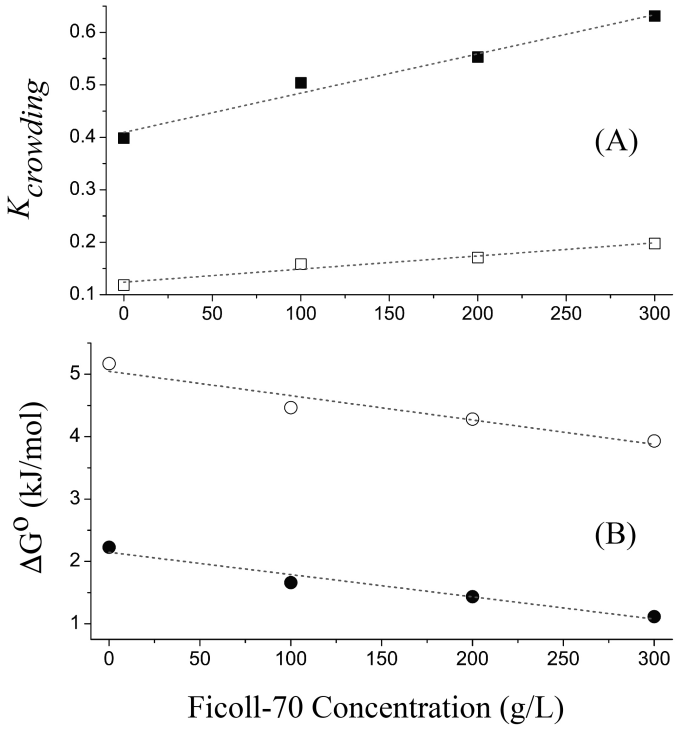

Figure 6: The Gibbs free energy changes (ΔG^0) of G12 crowding sensor depends on how the equilibrium constant is calculated using time-resolved fluorescence measurements as a function of crowding agent (Ficoll-70) concentration. (A) The equilibrium constant of G12 was calculated using both the amplitude ratios (α_1/α_2, black solid squares) and the fluorescence signal ($\alpha_1\tau_1/\alpha_2\tau_2$, open squares) emitted by each conformation according to the previously published time-resolved fluorescence on the G12 sensor [16]. (B) The corresponding (ΔG^0–value of G12 was also calculated using both approaches for estimating the equilibrium constant (α_1/α_2, black solid circles *versus* $\alpha_1\tau_1/\alpha_2\tau_2$, open circles). The dotted lines are shown here for eye guidance only with no theoretical basis.

Similar calculations were conducted on the G12 conformational thermodynamics ($K\ and\ \Delta G^0$) in response to Ficoll-70 concentration and the results are shown in Figure 6. As the concentration of the crowding agent (Ficoll-70) increases, the Gibbs free energy is reduced, which indicates a more favorable collapsed conformation of G12 in a crowded environment. In addition, the structure conformational equilibrium (stretched to collapsed) of these crowding sensors is not spontaneous (*i.e.*, $\Delta G^0 > 0$). It is therefore possible that our two-state model does not sufficiently account for the overall Gibbs free energy of the whole crowded mixture. Studies using nuclear magnetic resonance and fluorescence correlation spectroscopy have shown that crowding by Ficoll-70 or other common crowders (e.g., polyethylene glycol [PEG], dextran) can impact the thermodynamics of protein conformations [25-29]. Crowders impact the thermodynamic stability of domain movements [29], temperature-dependent proton exchange [26, 30], and protein unfolding [25, 28].

4.4 Changes in ΔG^o of Conformational Equilibrium of Environmental Sensors in Response to Ionic Strength and Crowding

The above mentioned results suggest that changes in the Gibbs free energy (ΔG^0) of these environmental sensors depends on the way the equilibrium constant is calculated using time resolved fluorescence. We propose to use a slightly different approach for examining the same experiment-based calculations in terms of the environmental ionic strength or crowding. For example, the changes in the ΔG^0 (i.e., $\Delta\Delta G^0$) due to ionic strength (e.g., KCl concentration) relative to the buffer (e.g., NaPi) can be written as following:

$$\Delta\Delta G^\circ = \Delta G^\circ\left(KCl\right) - \Delta G^\circ\left(NaPi\right) \tag{18}$$

Similarly, for crowding (Ficoll-70 concentration) effects on the changes in the ΔG^0 can be written as:

$$\Delta\Delta G^\circ = \Delta G^\circ\left(Ficoll\right) - \Delta G^\circ\left(PBS\right) \tag{19}$$

Figure 7 shows the changes ($\Delta\Delta G^0$) in the ΔG^0due to ionic strength (Figure 7A) and crowding (Figure 7B). Interestingly, the estimated $\Delta\Delta G^0$due to ionic strength (or KCl concentration) support the hypothesized conformational equilibrium (Figure 2A) between collapsed and stretched conformations of RD (Figure 7A). As the ionic strength increases, the $\Delta\Delta G^0$–value for RD conformational response decreases by approximately –3.5 kJ/mol over the 0 – 300 mM KCl range (Figure 7A). These findings support our stated hypotheses shown in Figure 2A.

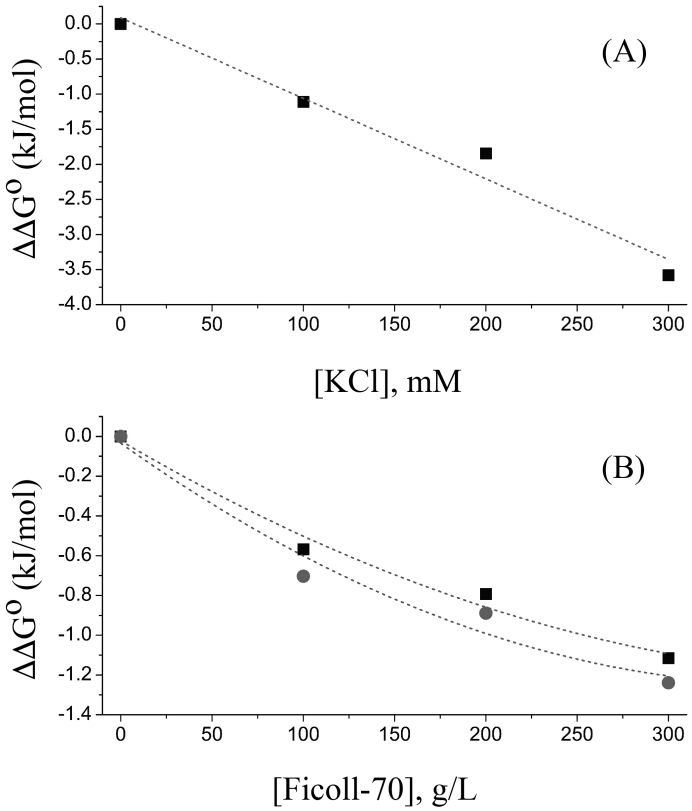

Figure 7: The relative changes ($\Delta\Delta G^o$) in Gibbs free energy change (ΔG^0) of environmental sensors with respect to buffer. (A) The relative change of Gibbs free energy changes ($\Delta\Delta G^0$) of RD sensor has negative values, which decreases as the KCl concentration (ionic strength) increases (i.e., spontaneous conformational changes that favors the stretched structure; Figure 2A). (B) The relative change of Gibbs free energy changes ($\Delta\Delta G^0$) of G12 sensor also exhibit negative values, which decreases as the Ficoll-70 concentration (crowding) increases (*i.e.,* spontaneous conformational changes that favors the collapsed structure; Figure 2B). Here, the – value seems less dependent on the way the equilibrium constant was calculated (solid squares: α_1/α_2; solid spheres: $\alpha_1\tau_1/\alpha_2\tau_2$).

In contrast, the $\Delta\Delta G^0$–value for G12 conformational response to crowding decreases only by approximately – 1.2 kJ/mol over the 0 – 300 g/L concentration range of Ficoll-70 (Figure 7B). Interestingly, the $\Delta\Delta G^0$–value for G12 due to crowding (Ficoll-70) seems less sensitive (within 10-20%) than $\Delta G^0$to how the equilibrium constant was calculated (*i.e.,* α_1/α_2 *versus* $\alpha_1\tau_1/\alpha_2\tau_2$) using time resolved fluorescence measurements. In contrast, the Gibbs free energy change (ΔG^o) of G12 in response to Ficoll-70 concentration (Figure 6B) is more sensitive to how the equilibrium constant was calculated (*i.e.,* α_1/α_2 *versus* $\alpha_1\tau_1/\alpha_2\tau_2$) with an estimated 66-70% difference. Importantly, the negative ($\Delta\Delta G^0$) values of RD (KCl) and G12 (Ficoll-70) indicate favorable and spontaneous conformational changes in response to the environment as described in Figure 2B. It is worth noting that this approach ($\Delta\Delta G^0$, equations 18 and 19) yields the same overall trend concerning the environmental-based energetics of the environmental sensors (i.e., RD, G12, G18, E6, and GE) investigated in this report.

5. CONCLUSIONS

We set out to investigate thermodynamic equilibrium and energetics associated with the conformational changes of selected mCerulean3-linker-mCitrine constructs, with variable amino acid sequences in the linker region, in response to both environmental ionic strength and macromolecular crowding. We provided a theoretical framework for using time-resolved fluorescence measurements to elucidate equilibrium constants and Gibbs free energy changes associated with structural conformations in response to the environmental ionic strength (potassium chloride, KCl) and crowding (Ficoll-70). Two approaches were discussed for calculating equilibrium constants using time-resolved fluorescence measurements of an ensemble of two different conformational distributions of donor-linker-acceptor constructs. Thermodynamic quantities were calculated for each environmental sensor as a function of either KCl (RD sensor with two oppositely charged alpha helices) or Ficoll-70 (G12, G18, E6, and GE with neutral alpha helices in the linker region with variable length and flexibility) concentrations and the number of amino acids in the linker region.

Using previously reported time-resolved fluorescence of RD [13], we calculated the corresponding equilibrium constant and the Gibbs free energy changes in NaPi buffer at room temperature. The calculated equilibrium constant was positive, and the corresponding negative estimated Gibbs free energy change suggests that the collapsed conformation of RD in a buffer is more favorable. This is attributed to the electrostatic interaction between the two oppositely charged alpha helices in the linker region. We then examined the thermodynamic equilibrium of RD in response to the environmental ionic strength in KCl solutions at room temperature. We found that the Gibbs free energy change decreases as ionic strength increases. This would suggest that the stretched conformation of RD will become more favorable as the environmental ionic strength increases.

Using fitting parameters from our previously published time-resolved fluorescence of G12, G18, E6, and GE sensors [16], we investigated the thermodynamics associated with these sensors in response to macromolecular crowding using Ficoll-70 as a crowding agent. We calculated the corresponding equilibrium constant and Gibbs free energy changes as a function of the amino acid sequence. The structure conformational equilibrium of the crowding sensors was found to be non-spontaneous due to positive estimated ΔG^0values. G12 and G18 have lower Gibbs free energy changes and suggest a more favorable collapsed conformation when compared with GE and E6, which agrees with the reported high FRET efficiency [16]. We hypothesize this trend is due to the shorter and more flexible linker region of G12 and G18. Calculations on G12 conformational thermodynamics (K and ΔG^o) in response to Ficoll-70 concentration showed that as the concentration of the crowding agent increases, the conformational Gibbs free energy changes (ΔG^0) is reduced, indicating a more favorable collapsed conformation of G12 in a crowded environment. However, the estimated ΔG^0–value depends on how time-resolved fluorescence measurements are used to calculate the corresponding equilibrium constant. We believe that the equilibrium constant (K) based on the amplitude ratio (*e.g.,* α_1/α_2 for crowding sensors, Figure 2B) in time-resolved fluorescence is more reliable due to the basic principles outlined above [22]. The structure conformational equilibrium of these crowding sensors is still non-spontaneous under crowded conditions.

To reconcile the differences in ΔG^o calculations based on the how the equilibrium constant is calculated (*e.g.,* α_1/α_2 *versus* $\alpha_1\tau_1/\alpha_2\tau_2$ for crowding sensors) using time-resolved fluorescence measurements, we calculated the relative changes in Gibbs free energy ($\Delta\Delta G^0$) with respect to the buffer in order to elucidate the ionic strength and crowding effects on the thermodynamic equilibrium of conformational changes of these environmental sensors. Our estimated $\Delta\Delta G^0$calculations indicate that ionic strength is more effective in causing favorable, spontaneous conformational changes in response to KCl concentration. Interestingly, the difference in the $\Delta\Delta G^0$–values of G12 seems less sensitive to the way we calculated the equilibrium constant using time-resolved fluorescence measurements.

ACKNOWLEDGEMENTS

The DNA of the sensors used here was a generous gift from Professor A. J. Boersma (Bijvoet Centre for Biomolecular Research, Utrecht University, Netherlands). We are thankful to Professor Martin Gruebele (University of Illinois, Urbana-Champaign) for useful discussion. The authors acknowledge the contributions of J. Schwarz, R.C. Miller, C.P. Aplin, and H.J. Leopold for the data collection, which was used here for the thermodynamics analysis. C. McCue and S.A. Mersch are grateful for the support provided by teaching assistantships from the Department of Chemistry and Biochemistry, University of Minnesota Duluth. S. Bergman acknowledges the support of the UROP and SURP programs at the University of Minnesota Duluth. E.D. Sheets and A.A. Heikal also acknowledge the Grant-in-Aid of Research, Artistry, and Scholarship program (GIA) award provided by the University of Minnesota.

REFERENCES

[1] H.-X. Zhou, "Polymer crowders and protein crowders act similarly on protein folding stability," *FEBS Lett.,* 587(5): 394 - 397 (2013).

[2] R. J. Ellis, "Macromolecular crowding: obvious but underappreciated," *Trends in Biochem. Sci.,* 26(10): 597 -604 (2001).

[3] G. Rivas, and A. P. Minton, "Macromolecular crowding *in vitro, in vivo*, and in between," *Trends in Biochem. Sci.,* 41(11): 970 - 981 (2016).

[4] J. Spitzer, and B. Poolman, "The role of biomacromolecular crowding, ionic strength, and physicochemical gradients in the complexities of life's emergence," *Microbiol. and Mol. Biol. Rev.,* 73(2): 371 - 388 (2009).

[5] T. Altamash, W. Ahmed, S. Rasool, and K. H. Biswas, "Intracellular ionic strength sensing using NanoLuc," *Int. J. Mol. Sci.,* 22(2): 677 - 288 (2021).

[6] E. Biemans-Oldehinkel, N. A. B. N. Mahmood, and B. Poolman, "A sensor for intracellular ionic strength," *Proc. Natl. Acad. Sci., USA,* 103(28): 10624 - 10629 (2006).

[7] B. Liu, C. Åberg, F. J. Van Eerden, S. J. Marrink, B. Poolman, and A. J. Boersma, "Design and properties of geneticallyencoded probes for sensing macromolecular crowding," *Biophys. J.,* 112(9): 1929 - 1939 (2017).

[8] B. Liu, S. N. Mavrova, J. van den Berg, S. K. Kristensen, L. Mantovanelli, L. M. Veenhoff, B. Poolman, and A. J. Boersma, "Influence of fluorescent protein maturation on FRET measurements in living cells," *ACS Sensors,* 3(9): 1735 - 1742 (2018).

[9] A. J. Boersma, I. S. Zuhorn, and B. Poolman, "A sensor for quantification of macromolecular crowding in living cells," *Nat. Methods,* 12(3): 227 - 230 , (2015).

[10] B. Liu, B. Poolman, and A. J. Boersma, "Ionic strength sensing in living cells," *ACS Chem. Biol.,* 12(10): 2510 - 2514 (2017).

[11] H. J. Leopold, R. Leighton, J. Schwarz, A. J. Boersma, E. D. Sheets, and A. A. Heikal, "Crowding effects on energy-transfer efficiencies of hetero-FRET probes as measured using time-resolved fluorescence anisotropy," *J. Phys. Chem. B,* 123(2): 379 - 393 (2019).

[12] M. Currie, H. Leopold, J. Schwarz, A. J. Boersma, E. D. Sheets, and A. A. Heikal, "Fluorescence dynamics of a FRET probe designed for crowding studies," *J. Phys. Chem. B,* 121(23): 5688 - 5698 (2017).

[13] R. C. Miller, C. P. Aplin, T. M. Kay, R. Leighton, C. Libal, R. Simonet, A. Cembran, A. A. Heikal, A. J. Boersma, and E. D. Sheets, "FRET Analysis of ionic strength sensors in the Hofmeister series of salt solutions using fluorescence lifetime measurements," *J. Phys. Chem. B,* 124(17): 3447 - 3458 (2020).

[14] C. Aplin, T. Kay , R. Miller , A. Boersma, E. Sheets, and A. Heikal, "Integrated fluorescence approach for FRET analysis of environmental sensors", *Proc. SPIE* 11122, *Ultrafast Nonlinear Imaging and Spectroscopy, VII* (2019).

[15] S. Mersch, M. Brink, R. Simonet, A. Boersma, E. Sheets, and A. Heikal, "Integrated laser-induced fluorescence spectroscopy of donor-linker-acceptor constructs for bioenvironmental sensing", *Proc. SPIE* 12228, *Ultrafast Nonlinear Imaging and Spectroscopy X* (2022).
[16] J. Schwarz, H. J Leopold, R. Leighton, R. C. Miller, C. P. Aplin, A. J. Boersma, A. A. Heikal, and E. D. Sheets, "Macromolecular crowding effects on energy transfer efficiency and donor-acceptor distance of hetero-FRET sensors using time-resolved fluorescence," *Methods and Appl. Fluoresc.,* 7(2): 025002 (2019).
[17] R. M. Clegg, "Förster resonance energy transfer—FRET what is it, why do it, and how it's done", *Laboratory Techniques in Biochemistry and Molecular Biology*, V33, *Chapter 1*, *Elsevier*, (2009).
[18] A. Zeug, A. Woehler, E. Neher, and Evgeni, "Quantitative intensity-based FRET approaches–A comparative snapshot," *Biophys. J.,* 103(9): 1821 - 1827 (2012).
[19] J. R. Lakowicz, "Principles of fluorescence spectroscopy", *3RD Edition*, *Springer US, Boston*, MA (2006).
[20] C. P. Aplin, R. C. Miller, T. M. Kay, A. A. Heikal, A. J. Boersma, and E. D. Sheets, "Fluorescence depolarization dynamics of ionic strength sensors using time-resolved anisotropy," *Biophys. J.,* 120(8): 1417 - 1430 (2021).
[21] T. M. Kay, C. P. Aplin, R. Simonet, J. Beenken, R. C. Miller, C. Libal, A. J. Boersma, E. D. Sheets, and A. A. Heikal, "Molecular brightness approach for FRET analysis of donor-linker-acceptor constructs at the single molecule level: A concept," *Front. Mol. Biosci., Biophys.*, 8:730394 (2021).
[22] M. R. Eftink, "Use of fluorescence spectroscopy as thermodynamics tool", *Methods Enzymol.*, V323: 459 - 473, *Academic Press*, (2000).
[23] I. Billard, and K. Lützenkirchen, "Equilibrium constants in aqueous lanthanide and actinide chemistry from time-resolved fluorescence spectroscopy: The role of ground and excited state reactions," *Radiochim. Acta,* 91(5): 285 - 294 (2003).
[24] O. Cañadas, A. Sáenz, G. Orellana, and C. Casals, "Equilibrium studies of a fluorescent tacrolimus binding to surfactant protein A," *Anal. Biochem.,* 340(1): 57 - 65 (2005).
[25] C. J. Stewart, G. I. Olgenblum, A. Propst, D. Harries, and G. J. Pielak, "Resolving the enthalpy of protein stabilization by macromolecular crowding," *Protein Sci.*, e4573 (2023).
[26] Y. Wang, M. Sarkar, A. E. Smith, A. S. Krois, and G. J. Pielak, "Macromolecular crowding and protein stability," *J. Am. Chem. Soc.,* 134(40): 16614 - 16618 (2012).
[27] N. Das, and P. Sen, "Macromolecular crowding effect on the structure, function, conformational dynamics and relative domain movement of a multi-domain protein as a function of crowder shape and interaction," *Phys. Chem. Chem. Phys.*, 24: 14242 (2022).
[28] N. Das, and P. Sen, "Shape-dependent macromolecular crowding on the thermodynamics and microsecond conformational dynamics of protein unfolding revealed at the single-molecule level," *J. Phys. Chem. B,* 124(28), 5858-5871 (2020).
[29] S. Biswas, J. Kundu, S. K. Mukherjee, and P. K. Chowdhury, "Mixed macromolecular crowding: a protein and solvent perspective," *ACS omega,* 3(4): 4316 - 4330 (2018).
[30] A. C. Miklos, C. Li, N. G. Sharaf, and G. J. Pielak, "Volume exclusion and soft interaction effects on protein stability under crowded conditions," *Biochem.,* 49(33): 6984 - 6991 (2010).